Simulation of signal induction in the Caliste-SO detector

A. Barylak*[,a], J. Barylak[a], T. Mrozek[a,b], P. Podgórski[a], M. Stęślicki[a], D. Ścisłowski[a]

[a]Space Research Center of Polish Academy of Sciences, Poland,

[b]Astronomical Institute, University of Wrocław, Poland

ABSTRACT

The paper presents a two methods for simulation of signal induction in the detector. First method base on carriers tracks calculation while second method include simplification of accelerating calculations. Calculation has been performed for Caliste-SO detector, which is cadmium telluride X-ray detector. This detector will be used in the Solar Orbiter/STIX instrument. Solar Orbiter is M-class mission of the ESA's programme Cosmic Vision 2015-2025, which is conducted in collaboration with NASA. It will be launched in October 2018. STIX (Spectrometer/Telescope for Imaging X-Rays) is X-ray telescope and spectrometer and will observe solar X-ray emission from 4 to 150 keV using Fourier-imaging technique. Deep space condition can influence significantly the detector parameters. Tools for detectors behaviour analysis are needed to understand how this harsh radiation environment can influence detector quantum efficiency.

Keywords: Caliste-SO, signal induction, X-ray detector, detector ageing, CdTe

1. INTRODUCTION

Solar Orbiter (SO) [1] is M-class mission of ESA's Comic Vision 2015-2025 and NASA. The main objective of SO is to investigate the connection between the Sun and the heliosphere. To achieve this objective, a combination of telescopic observations and in-situ measurements will be performed. The satellite will come close to the Sun for 0.3 AU on the heliospheric orbit. Launch of the mission is planned in October 2018.

Spectrometer/Telscope for Imaging X-Rays (STIX) [2] is one of scientific instruments on-board the SO. The instrument will provide imaging spectroscopy of solar X-ray emission from 4 to 150 keV with unprecedented spatial resolution due to close proximity to the Sun. The STIX is a Fourier imager. This imaging technique was used successfully in other instruments in the past like e.g. Hard X-ray Telescope (HXT) [3] on the Japanese mission Yohkoh and in the Reuven Ramaty High Energy Solar Spectroscopic Imager (RHESSI) [4]. The STIX imager consist with 32 pairs of grids which allows to map the direction of X-ray photons. Behind each pair of grids, Caliste-SO X-ray detector [5] is placed.

The Caliste-SO utilize cadmium telluride (CdTe) semiconductor sensors to detected X-rays photons, such detectors are increasingly used in modern satellite observatories [6]. Comparing to traditional materials (like silicon and germanium) used in previous high energy spectrometers, CdTe provides good detection efficiency and high performance in room temperatures. The capability of CdTe detectors in X-rays imaging applications has already been demonstrated with the

* Corresponding author. E-mail: abarylak@cbk.pan.wroc.pl

Photonics Applications in Astronomy, Communications, Industry, and High-Energy Physics Experiments 2015, edited by Ryszard S. Romaniuk, Proc. of SPIE Vol. 9662, 966217 · © 2015 SPIE
CCC code: 0277-786X/15/$18 · doi: 10.1117/12.2205731

INTErnational Gamma-Ray Astrophysics Laboratory (INTEGRAL) satellite, which operates, on high eccentric orbit (9000 – 154 000 km), almost 13 years [7].

Analysis of INTEGRAL data shows that detector parameters getting worse during mission, because instrument's detectors are exposed on Cosmic Radiation. Solar energetic particles streams are also dangerous for detector performance [8]. Sharp drop in detector's parameters was observed due to November 2003 giant solar flare [7]. Detectors ageing effect is well illustrated by the performance of RHESSI [9] X-ray solar observatory. This instrument operates on low Earth's orbit over 13 years and use germanium detectors to register X-rays of solar origin. RHESSI detectors experience noticeable degradation under the influence of charged particles from the Earth's radiation belts.

One of methods of monitoring detectors ageing is to measure radiation from radioactive calibration source [10, 11]. Detectors parameters can be estimated by measuring widths and intensities of lines produced by the radioactive source. It has been successfully demonstrated that detector damages can be annealed out on time scales of days to weeks [8,11]. In-flight annealing can restore detectors parameters to original values. To predict how Cosmic Radiation will influence detector parameters, a pre-launch accelerator tests will be performed in which proton streams will be used to irradiate detectors [7].

Spectra registered by STIX will be send to the Earth with limited resolution because the SO is a deep space mission which causes telemetry restrictions. That limits the usefulness of radioactive source in measuring detectors parameters. A remedy for this is to develop complete simulation tool for reconstruction detector response matrix (DRM) with various input parameters. This tool should be able to reconstruct precisely spectra of radioactive sources measured with Caliste-SO in laboratory. Thus, we can be sure that our understanding of detector is good enough to estimate its performance from measurements conducted during the interplanetary mission.

One of effects ongoing during photon registration is the signal induction in the detector. It is very important in prediction of ageing effect because it depends on crystal effects depending on detector characteristics. In this paper, we will show two methods of calculation of signal induction in the detector with various crystal effects implemented.

2. CALISTE-SO DESCRIPTION

The Caliste-SO detector contain a 10×10 mm^2 area CdTe sensor with thickness of 1 mm and a dedicated front-end electronics. This hybrids are manufactured in 3D Plus technology [5]. There are four printed circuit boards in the electronic part of Caliste-SO. One is for ASIC, two containing discrete parts for power supply filtering and local decoupling, and one is for routing the sensor high bias voltage. Bias voltage of 200 V is used to obtain good charge collection. To obtain good spectral resolution, a blocking Schottky contact is used on the anode. It limits the leakage current. Acrorad, Japan, produced CdTe sensors. Pixel structure on the anode is made in the Paul-Scherrer Institute, Switzerland, and crystals are integrated with electronics by CEA Sacley, France.

2.1. CdTe properties

The CdTe material have high average atomic number of 50, high photoelectric absorption coefficient, and high density of 5.58 g/cm^2 in relation to other materials used in X-ray detectors. In result, it is suited material for spectroscopic detection of X-rays.

However, CdTe growth process is not easy and the quality of crystals is worse than silicon and germanium crystal. A lot of structural defects are formed during growth process and in result, material have relatively poor carrier transport properties. The biggest problem is short lifetime of holes in comparison with the drift time through crystal of millimetre thickness. Significant charge loss occurs for higher energy of photon absorption. Table 1 contain the mobility and the lifetime of electrons and holes calculated in room temperatures.

Table 1. Charge carriers parameters of CdTe crystal.

Carrier type	Mobility ($cm^2/(Vs)$)	Lifetime (μs)
Electron	1100	3
Hole	100	1

2.2. Electrodes

The cathode, on the top of the detector (the side on which X-rays falls), is made from monolithic platinum electrode with a thickness of 16 nm. Platinum have similar to p-type CdTe (about 5.6 eV) work function, which equal 5.4 eV. In result, nearly Ohmic contact is formed, which pass carriers easily.

The anode contain three layer: gold, titanium and aluminium. The work function of the innermost aluminium layer equal 4.2 eV and is much lower than that of CdTe. It forms a Shottky contact and blocks majority of hole carriers. The gold layer is for the protection of anode, and titanium layer, which is between gold and aluminium, is for better adhesion of the two other metals.

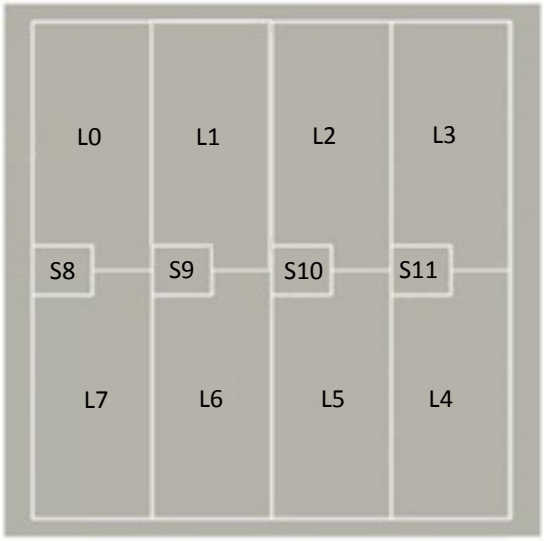

Figure 1. Pixel pattern of the Caliste-SO anode.

The originally monolithic anode is divided into 8 big and 4 small pixels by etching. Around this pattern is also etched guard ring that eliminates the adverse effects occurring at the detector edge and prevents surface leakage current along the edges of the crystal to influence the pixels. Pixels are arranged in four strips, which is required for detection of Moiré pattern projected by pair of grids. The additional use of two large and one small pixel in the one strip allow to change the effective area according to incoming photon rate. In result, it will be possible to limit pulse pile-up and dead-time by disabling pixels. The gap between pixels on anode is 50 μm, and 75 μm on the outside of the guard ring

3. FIRST METHOD

First method described in this work was presented in paper of Ch. Xu, M. Danielsson and H. Bornefalk [12]. It consists of electric field calculation, determination of the charge carriers tracks and signal shape calculation using Shockley-Ramo theorem. Einstein theory of Brownian motion and diffusion was used to compute charge diffusion.

3.1. Field simulation

The electric potential φ in the detector volume can be found by solving the Poisson equation:

$$\nabla^2\varphi(\vec{r}) = -\frac{\rho(\vec{r})}{\varepsilon}$$

on a three-dimensional grid, where ε is the material permittivity and $\rho(r)$ is the charge density distribution. The electric field E then follows from:

$$\vec{E}(\vec{r}) = -\nabla\varphi(\vec{r})$$

The space-charge in the bulk has to be known to determine the electric potential distribution. This in turn depends on the electric field. Applied voltage in Caliste-SO is sufficiently high that all mobile charge are swept out. In result, the effective doping concentration determines the space charge, which is constant in whole crystal and equal -0.029 C/m^3.

This issue was solved in COMSOL ver. 4.0. The anodes of CdTe detector are grounded at zero potential and the cathode is put 200 V. Neumann boundary condition was applied to the region between electrodes. Fig. 2 show the electric potential distribution for the cross section through big pixel in Caliste-SO.

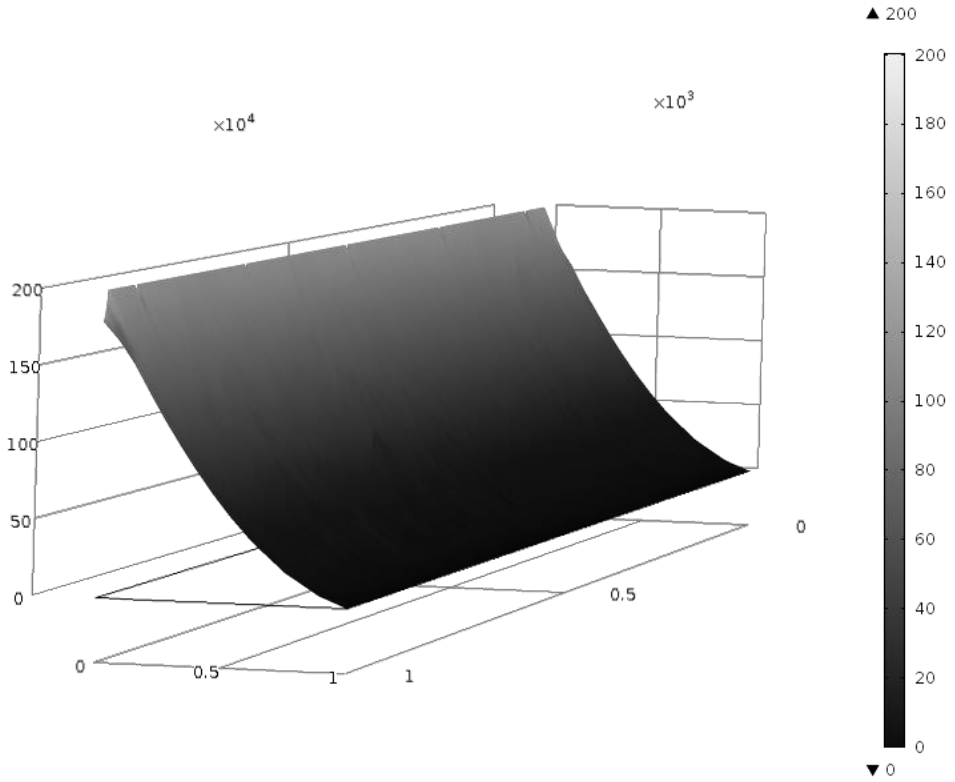

Figure 2. Electric potential in the cross section of pixels volume in detector.

Weighting field is needed to evaluate induced current on electrode. It describes the electrostatic coupling between moving charges and investigated electrodes. We calculate them also in COMSOL using Laplace's equation. Potential of the investigated electrode must be set on 1 V and other electrodes must be grounded. Each electrodes has its own weighting potential. Fig. 3 show the weighting potential of single big pixel in cross section.

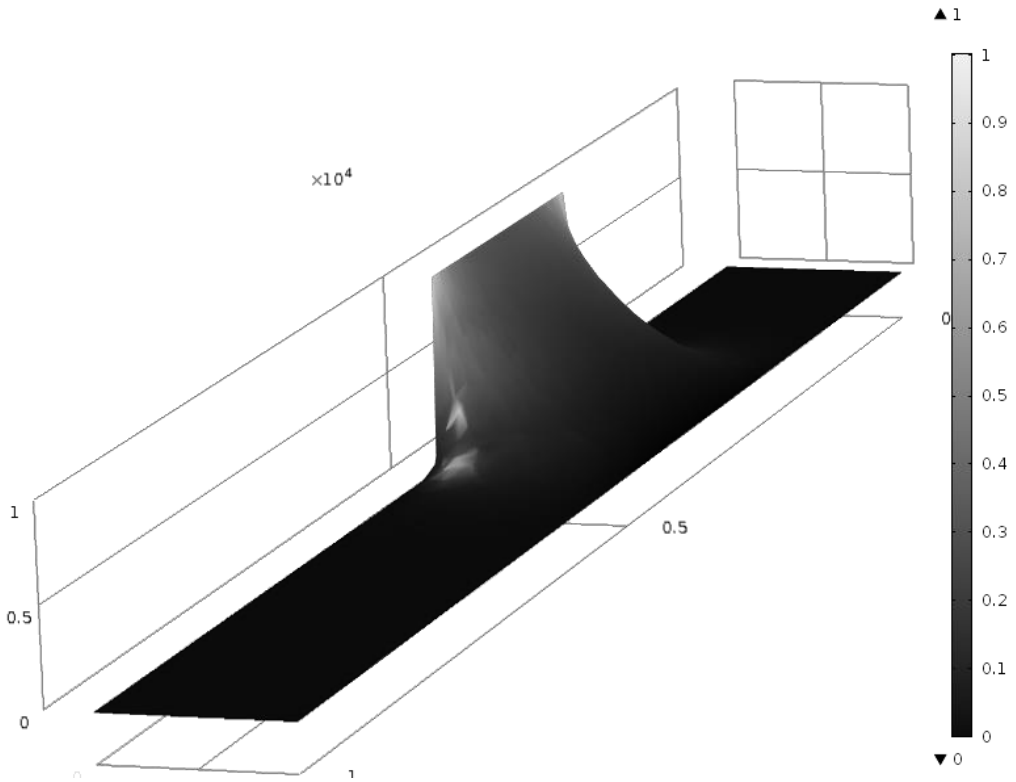

Figure 3. Weighting potential in the cross section of pixels volume in detector.

3.2. Charge drift

A lot of charges are generated by single photon absorption. For a given electric field they have a constant speed instead of accelerating because they are braking during repeated collisions with the crystal lattice. Each carrier is separately simulated. The drift velocity of charge carriers is the product of mobility and electric field:

$$\vec{v}_d = \mu\vec{E}$$

The charges diffuse during charge-collection process. In result, the charge cloud grows. This effect is described by Einstein theory that give diffusion equation:

$$P(dx) = \frac{1}{\sqrt{4\pi D dt}} e^{-\frac{dx^2}{4Ddt}}$$

where *dx* is the diffusing distance of a carrier in one direction, which is randomly selected from the Gaussian probability distribution $P(dx)$ in a simulation time step dt. D is the diffusion coefficient calculated from equation

$$D = \frac{\mu k T}{q}$$

k is the Boltzmann constant and *T* is a temperature in Kelvin scale. The diffusion distance is calculated separately for each direction and the diffusion velocity $\vec{v}_f$ is calculated from:

$$\vec{v}_f = \frac{d\vec{r}_f}{dt}, \qquad d\vec{r}_f = (dx, dy, dz)$$

Finally, the overall velocity is a sum of two components:

$$\vec{v}_i = \vec{v}_d + \vec{v}_f$$

We do not take into account Coulomb interaction between charge carriers because of Coulomb force is much smaller than force coming from electric field.

3.3. Signal generation

During movement of the carriers, current on the readout electrodes is induced. It can be calculate from Shockley-Ramo theorem [13]. The current induced on an electrode follows from:

$$i(t) = -q\vec{E}_w(\vec{r}(t))\vec{v}_i(t)$$

Where $\vec{E}_w$ is weighting field of investigated electrode and *t* is the drift time.

There are many structural defects in CdTe detectors. This requires inclusion of charge trapping effect to simulation. In result, current is expressed as:

$$i(t) = -qe^{-\frac{t}{\tau}}\vec{E}_w(\vec{r}(t))\vec{v}_i(t)$$

where τ is the mean life time of the charge carriers. Currents are calculated separately for each charge. To obtain total signal induced on the electrode, we must sum currents from all charge carriers.

The charge collected on the electrode can be obtained by integrating the induced current in time.

4. SECOND METHOD

Second method [14] bases on slightly simplified approach. Firstly, electric field is considered as perpendicular to electrodes faces. Secondly, carriers trajectories are not calculated. Thirdly, current induced on an electrode is not calculated, only charge collected on the electrode is calculated.

4.1. Electric field in crystal

The gaps between electrodes are very small compared to the crystal thickness. Therefore, the electric field lines inside the crystal are nearly perpendicular to the electrodes plane except guard ring. The field lines are assumed to be exactly along *x* coordinate. Guard ring is of no interest. In result, Poisson's equation is:

$$\frac{\partial^2 U(x)}{\partial x^2} = -\frac{\rho}{\epsilon_r \epsilon_0} \quad \Longrightarrow \quad U(x) = -\frac{\rho}{2\epsilon_r \epsilon_0}\, x^2 + C_1 x + C_2$$

where C_1 and C_2 are integration constants, which can be calculated from the boundary condition *U(0) = V* and *U(d) = 0*. *V* is voltage applied to the cathode. The potential is thus:

$$U(x) = -\frac{\rho}{2\epsilon_r \epsilon_0}\, x^2 + \left(\frac{\rho d}{2\epsilon_r \epsilon_0} - \frac{V}{d}\right) x + V$$

and electric field:

$$E(x) = -\frac{\partial U(x)}{\partial x} = -\frac{2V_d}{d^2} x + \frac{V_d - V}{d}, \quad V_d = \frac{\rho d^2}{2\epsilon_r \epsilon_0}$$

V_d is depletion voltage. At smaller voltages than V_d some portion of CdTe crystal is undepleted, and detector will lose sensitivity in particular for low-energy X-rays.

4.2. Charge drift

Time of charge drift as a function of distance can be calculated from equation on drift speed in electric field:

$$t(x) = \int_{x_0}^{x} \frac{dt}{dx'} dx' = \int_{x_0}^{x} \frac{1}{\mu E(x')} dx' = \frac{d^2}{2\mu V_d} \ln \frac{V - V_d + 2V_d \frac{x}{d}}{V - V_d + 2V_d \frac{x_0}{d}}$$

where x_0 is start location, and d is crystal depth.

For considered voltages *V* = -200 *V* and V_d = -150 *V* the calculated time of charge drift through entire crystal along *x* axis amounts to about 60 *ns* for electrons, and over ten times longer for holes.

4.3. Diffusion

Electric field is considered as perpendicular to the electrodes. While charges move along direction of the field the charge cloud expands. Diffusion along field direction does not affect the induced signal significantly and can be neglected. Therefore, the charge can be modelled 2-dimensional in *y*-*z* plane for each position of *x*.

The diffusion of charge cloud is calculated from Fick's second law:

$$\frac{\partial \Phi(\vec{r}, t)}{\partial t} = D\nabla^2 \Phi(\vec{r}, t), \quad \Phi(\vec{r}, t) = \frac{1}{\left(\sqrt{2\pi}\sigma(t)\right)^3} e^{-\frac{\vec{r}^2}{2\sigma(t)^2}}$$

where, $\Phi(\vec{r}, t)$ is normalized spherical Gaussian distribution of charge cloud density. Standard deviation $\sigma(t)$ can be calculated by inserting the distribution to Fick's second law equation. In result:

$$\sigma(t) = \sqrt{2Dt}$$

D is diffusion constant, given by Einstein relation:

$$D = \frac{|\mu| kT}{e}$$

where *k* is the Boltzmann constant, *T* is the absolute temperature and *e* is elementary charge.

Finally, diffusion width as a function of distance is:

$$\sigma(x) = d \sqrt{\frac{kT}{eV_d} \ln \left(\frac{V - V_d + 2V_d \frac{x}{d}}{V - V_d + 2V_d \frac{x_0}{d}} \right)}$$

The relation does not depend on mobility μ. For *V* and V_d voltages as considered in previous section and for temperature of 253 K, the diffusion width is equal to 18 μm. It is smaller than gaps between pixels.

4.4. Signal generation

In this method, the current as function in time is not calculated. Only total charge induced on the electrodes is calculated from Shockley-Ramo theory [13]. This equation follows:

$$\Delta Q_k = Q(\psi_k(\vec{r}_{start}) - \psi_k(\vec{r}_{end}))$$

Using this equation simplifies the calculations significantly.

4.5. Charge carrier losses

The charge carrier losses can be included in this method in the same way as previously. The number of carriers $n_e(t)$ and $n_h(t)$ after time t can be calculated from exponential relation knowing the lifetimes of the charge carriers:

$$n_e(t) = n_0 e^{\frac{-t}{\tau_e}}, \quad n_h(t) = n_0 e^{\frac{-t}{\tau_h}}$$

where τ_e is lifetime of electrons and τ_h is lifetime of holes. n_0 is the initial number of electrons and holes.

4.6. Simulation flow

Simulation proceeds in following steps:

1. Calculation of the time-position relation $t(x)$.
2. Determination of the diffusion width $\sigma(x)$.
3. Integrating the product of charge distribution over planes parallel to the electrodes and weighting field.
4. Subtracting the weighting field at the start location.
5. Applying time-position equation to transform induced signal from position domain to time domain.
6. Applying charge losses to time-dependent signal on the electrodes.
7. Summing the contributions from electrons and holes.

5. RESULTS OF BOTH METHODS

Induced charge as functions of time are shown in Fig. 4 for three interaction depths: near cathode (x = 0.1 mm), in the middle (x = 0.5 mm) and near anode (x = 0.9 mm). The absorption occurs near the centre of pixel L5. The signal is normalised to the total charge created in result of photon interaction. Each function has fast-rising part corresponding to signal induced by electrons and slow-rising part corresponding to signal induced by holes. Charge collection lasts longer when interaction occurs deeper due to lower mobility of holes and their longer way. Additionally, hole losses increase with the drift time thus the final values of relative influenced charge are smaller.

Fig. 5 shows signal induced on electrodes over pixel L4 in case where interaction took place within adjacent pixel L5 near to the boundary between the pixels. The selected distance of 100 μm between the interaction and the pixel boundary is much greater than charge diffusion width, so that the diffusion influence can be neglected. Signal induced within pixel L5 is similar to previous case shown in Fig. 4. The sharp drop of signal induced within pixel L4 arises from its weighting field profile. Negative part of the signal induced by holes occurs only for interactions close to the anode. In such case the final value of relative influenced charge remains negative since some portion of holes is trapped during collection.

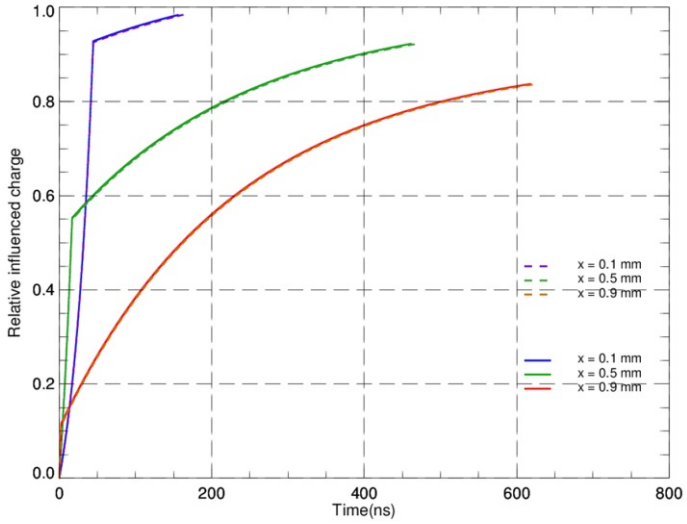

Figure 4. Signal induced within pixel L5 for different interaction depths near the centre of the pixel. Results obtained by first method are marked with solid line and second method with dashed line.

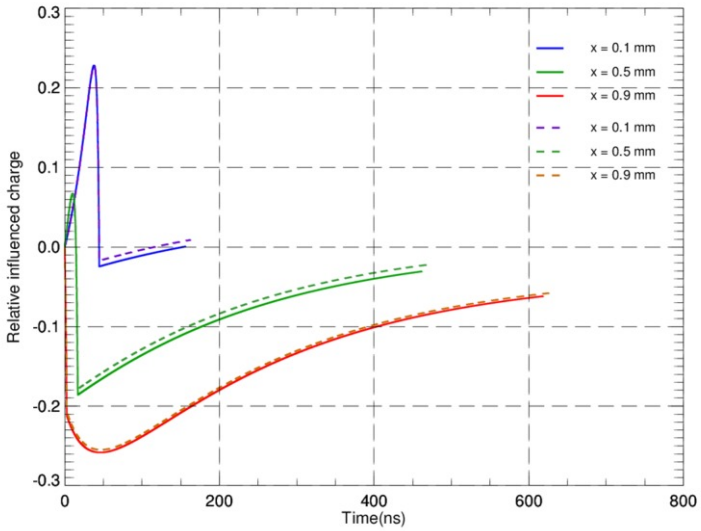

Figure 5. Signal induced within pixel L4 as result of interaction within pixel L5 located 100 μm from geometric boundary between pixels L4 and L5 at different depths. Results obtained by first method are marked with solid line and second method with dashed line.

6. DETECTOR EFFECTIVITY

Effectivity of Caliste-SO as function of the interaction depth and the lifetime of carriers is shown in Fig.6. The carrier lifetime is the percentage of initial lifetime, because we expect that this parameters will decrease during mission. The effectivity remains almost unchanged even when the lifetime drops to the 30% of its initial value for interactions near cathode. Low energy photon are absorbed in this region. Therefore, low energy part of spectra will be longer unaffected. Effectivity for low energy photons drops rapidly starting from the 20% of carrier lifetime. High energy part of spectra gradually decrease with decreasing lifetime.

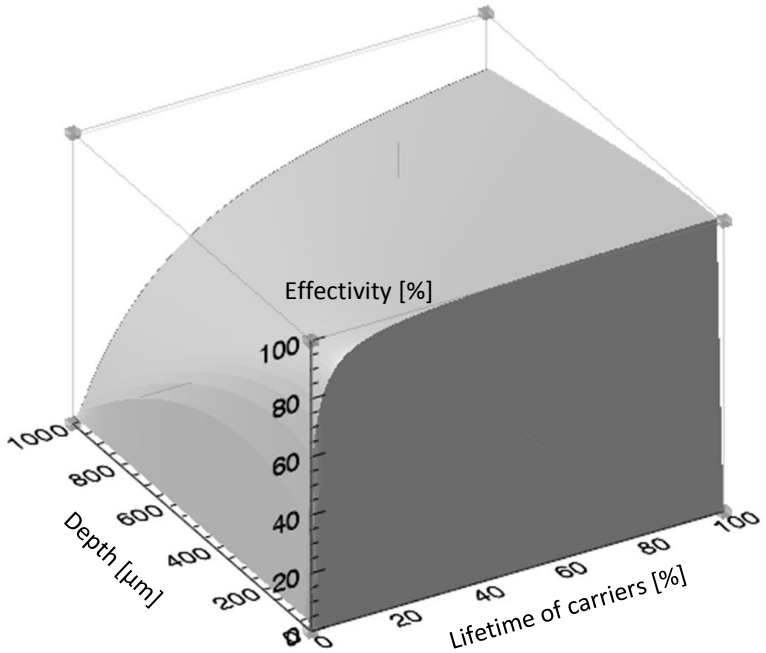

Figure 6. Effectivity of detectors as function of the interaction depth and the lifetime of carriers level.

7. SUMMARY

This simulation can be used to produce set of DRMs with different lifetime of carriers. Using these DRMs, we can find one which produce correct signal from radioactive source. This allow us to estimate current detectors parameters. Such DRMs can be constructed through combination of Geant4 simulation showed in [15] and signal simulation presented in this paper.

Both methods are in good agreement. One of the advantages of the second method is that it is faster. It do not calculate tracks in small time step. However, first method can be used to calculate charge sharing between pixels and to investigate edge of the crystal. Charge sharing is very important effect because it generates double counts. This events will be rejected by the STIX electronics, therefore it influence the observed spectra shape. On the other hand, the maximal diffusion length is much lower than size of pixels. It seems that this effect is marginal and can be neglected. Double counting occurs also when secondary photon is absorbed in adjacent pixel. This kind of effects can be estimate by Monte Carlo simulation described in [15].

This simulation can be used also as a part of whole STIX instrument simulations, which contain software simulations of X-ray sources, imaging instrument and hardware components such as detector simulator [16] and on-board computer. This simulations will allow to better understand response of the instrument. Also will be possible to take into account various effects such as pile-up, dead time or even secondary radiation from mechanical components of the instrument. All this effects influence measured data.

Acknowledgement

This work was supported by Polish National Science Centre grant 2011/01/M/ST9/06096.

REFERENCES

[1] Müller, D., et al., "Solar Orbiter. Exploring the Sun-Heliosphere Connection", Sol. Phys. 285, 25-70, (2013).

[2] Benz, A. O., et al., "The Spectrometer Telescope for Imaging X-rays (STIX) on board the Solar Orbiter mission", Proc. SPIE 8443, 131, (2012).

[3] Kosugi, T., et al., "The Hard X-ray Telescope (HXT) for the SOLAR-A Mission", Sol. Phys. 136, 17-36, (1991).

[4] Lin, R. P., et al., "The Reuven Ramaty High-Energy Solar Spectroscopic Imager (RHESSI)", Sol. Phys. 210, 3-32, (2002).

[5] Meuris, A., et al., "Caliste-SO X-ray micro-camera for the STIX instrument on-board Solar Orbiter space mission", Nucl. Instrum. and Meth. A 695, 288-292, (2012).

[6] Del Sordo S., et al., "Progress in the development of CdTe and CdZnTe semiconductor radiation detectors for astrophysical and medical applications", Sensors 9, 3491-3526, (2009).

[7] Lebrun, F., "The ISGRI CdTe gamma camera In-flight behaviour", Nuclear Science Symposium Conference Record, 2004 IEEE, 7, 4373-4377, 16-22 Oct. (2004).

[8] Owens, A., et al., "An assessment of radiation damage in space-based germanium detectors due to solar proton events", Nucl. Instrum. and Meth. A 583, 285-301, (2007).

[9] Smith, D., Lewis, M., "RHESSI's Anneal Adventure", RHESSI Nuggets 127, (2010).

[10] Terrier, R., et al., "In-flight calibration of the ISGRI camera", Astron. & Astrophys. 411, L167-L172, (2003).

[11] Albernhe, F., et al., "Degradation and recovery of Ge detectors: tests prior to a space mission", Nucl. Instrum. and Meth. A 492, 91-96, (2002).

[12] Xu, Ch., et al., "Evaluation of Energy Loss and Charge Sharing in Cadmium Telluride Detectors for Photon-Counting Computed Tomography", IEEE Trans. on Nucl. Science 58, 3, (2011).

[13] He, Z., "Review of the Shockley-Ramo theorem and its application in semiconductor gamma-ray detectors", Nucl. Instr. Meth. A 463, 250-261, (2001).

[14] Grimm, O., (2014), private communication.

[15] Barylak, J., et. al., "Geant4 simulations of detector response matrix for Caliste-SO", Proc. SPIE 9290, 929037 (2014).

[16] Podgórski, P., et. al., "Hardware simulator of Caliste-SO detectors for STIX instrument", Proc. SPIE 8903, 89031V (2013).